HCMV exploits STING signaling and counteracts IFN and ISG induction to facilitate dendritic cell infection

Bibiana Costa
TWINCORE, Centre for Experimental and Clinical Infection Research
Jennifer Becker
Center for Experimental and Clinical Infection Research
Tobias Krammer
Institute for RNA-based Infection Research (HIRI) https://orcid.org/0000-0002-7638-9476
Felix Mulenge
TWINCORE, Centre for Experimental and Clinical Infection Research
Verónica Durán
TWINCORE, Centre for Experimental and Clinical Infection Research
Andreas Pavlou
Hannover Medical School
Xiaojing Chu
University Medical Center Groningen
Yang Li
Helmholtz Centre for Infection Research https://orcid.org/0000-0003-4022-7341
Luka Cicin-Sain
Helmholtz Centre for Infection Research https://orcid.org/0000-0003-3978-778X
Britta Eiz-Vesper
Hannover Medical School
Lars Dolken
Julius-Maximilians-University Würzburg https://orcid.org/0000-0002-4651-3544
Antoine-Emmanuel Saliba
Helmholtz Institute for RNA-based Infection Research https://orcid.org/0000-0001-8539-2784
Florian Erhard
University of Wuerzburg https://orcid.org/0000-0002-3574-6983
Ulrich Kalinke
Ulrich.Kalinke@twincore.de

TWINCORE, Centre for Experimental and Clinical Infection Research https://orcid.org/0000-0003-0503-9564

Article

Keywords:

Posted Date: January 13th, 2022

DOI: https://doi.org/10.21203/rs.3.rs-953016/v1

Additional Declarations: There is **NO** Competing Interest.

Version of Record: A version of this preprint was published at Nature Communications on February 26th, 2024. See the published version at https://doi.org/10.1038/s41467-024-45614-3.

Abstract

Human cytomegalovirus (HCMV) is a widespread obligatory human pathogen causing life-threatening disease in immunocompromised hosts. Myeloid cells such as monocyte-derived dendritic cells (moDCs) are targets of HCMV. Here, we performed single-cell RNA sequencing, which revealed infection of most moDCs upon *in vitro* HCMV exposure, whereas only a fraction of them initiated viral gene expression. We identified three moDC subsets, of which $CD1a^{-}/CD86^{-}$ cells showed the highest susceptibility. Upon HCMV entry, STING activation not only induced IFN-β, but also promoted viral gene expression. Upon progression of infection, IFN-β but not IFN-λ1 expression was inhibited. Similarly, ISG expression was initially induced and then shut off and thus allowed productive infection. Increased viral gene expression was associated with the induction of several pro- (*RHOB, HSP1A1, DNAJB1*) and anti-viral (*RNF213, TNFSF10, IFI16*) genes. Thus, moDC permissiveness to HCMV depends on complex interactions between virus sensing, regulation of IFNs/ISGs and viral gene expression.

Introduction

Human cytomegalovirus (HCMV) is a human-specific β-herpesvirus with a prevalence of 40-90% in the human population. While in immunocompetent hosts HCMV infection mostly is asymptomatic, immunocompromised individuals may develop life-threatening disease. Furthermore, HCMV is the leading cause of congenital disabilities [1]. Myeloid cells are natural targets of both lytic and latent HCMV infection *in vivo* and represent an important viral reservoir [2,3]. Monocytes are recruited from the blood to sites of inflammation, where they differentiate to macrophages and/or dendritic cells (DCs) [4,5]. DCs prime and re-stimulate HCMV-specific T cells and are important producers of interferons (IFN), which induce the expression of anti-viral IFN-stimulated genes (ISGs) that protect the host from severe HCMV infection [6]. HCMV evades and exploits DC functions [7] and encodes several proteins dedicated to evade IFN responses which are expressed throughout the viral life cycle, such as *UL122* and *UL123, US9, UL31* (reviewed in [8]) and *UL145* [9]. Some of them target the cytosolic cGAS/STING axis that is involved in the induction of IFN responses upon HCMV infection of monocyte-derived dendritic cells (moDCs) [10]. Furthermore, HCMV virions contain proteins, viral coding and non-coding RNAs as well as host mRNAs that can influence host cells directly upon viral entry [11–13].

In many studies, HCMV mediated immune evasion was addressed in highly permissive fibroblast cell lines [14]. While single-cell RNA sequencing (scRNA-seq) analysis of such cells provided information about the complex expression kinetics of viral genes [15], these experiments do not allow conclusions about HCMV infected primary end-differentiated and non-cycling myeloid cells. Myeloid cells are generally less susceptible to HCMV infection than fibroblasts. A recent study revealed that permissiveness was not determined by viral entry [16] implying that some cellular factors were responsible.

Here we aimed to uncover factors that facilitate efficient HCMV infection in moDCs by scRNA-seq. We identified three distinct moDC subsets with different infection susceptibilities. The in-depth analysis of

virion-associated transcripts confirmed that upon exposure to HCMV most cells are infected, whereas only a few support productive viral gene expression. Our findings indicate that initiation of immediate early (IE) viral gene expression is induced upon STING activation and thus correlates with *IFNB1* expression. Upon progression of HCMV infection, *IFNB1* but not *IFNL1* expression is inhibited and ISG expression is shut off. Moreover, we identified pro- and anti-viral candidates that are associated with increased HCMV gene expression in moDCs. In conclusion, we reveal a complex interaction network between IFN induction, ISG modulation, and initiation of viral gene expression that governs the outcome of HCMV infection in moDCs.

Results

Single-cell RNA sequencing highlights moDC heterogeneity

Upon exposure with recombinant HCMV expressing NeonGreen (HCMV-NG) coupled to the IE1 (*UL123*) protein [17], only a minority of moDCs showed NG expression (Fig. 1a and Supplementary Fig. 1a). To address whether certain transcriptomic profiles determined HCMV permissiveness of moDCs, we studied the heterogeneity of moDCs exposed to HCMV-NG after 8 h of incubation by scRNA-seq. To minimize batch effects, mock- and HCMV-NG exposed cells were labeled with tagged anti-CD45 and anti-HLA-DR antibodies, respectively, and pooled prior to scRNA-seq (Fig. 1b). Both antibodies carried specific DNA oligo tags. The presence of antibody-derived tags (ADT) was used to de-multiplex cells [18]. moDCs from two donors were infected each with two independently produced HCMV-NG preparations (V1, V2). Accordingly, data from a total of four separate runs with overall 18,936 cells that passed quality control were combined, analyzed by unsupervised clustering and visualized using non-linear dimensionality reduction (Supplementary Fig. 1b). CD45-ADT$^+$ (Fig. 1c) and HLA-DR-ADT$^+$ cells (Fig. 1d) clustered separately. Each ADT-labeled subset segregated into several clusters, which were primarily defined by variations in host gene expression (Supplementary Fig. 1c). Amongst HCMV-NG exposed cells, only one cluster showed strong expression of *UL123* as well as of many other viral RNAs (Fig. 1e and Supplementary Fig. 1d). Accordingly, we defined three groups of moDCs, “mock-exposed” cells (M) that were not exposed to the virus, “bystander” cells (B) that were HCMV-NG exposed but did not show strong viral gene expression (Fig. 1e), and “productively infected” cells (P) that showed high viral RNA levels including *UL123*. Samples segregated according to the donor origin of the moDCs, whereas batch effects between runs and virus preparations used were minimal (Supplementary Fig. 1b). For further analysis, single clusters that were composed of cells from both donors were manually split according to the donor origin. As a result, moDCs of each donor comprised three mock-exposed clusters (M1-3, CD45-ADT$^+$), four to five bystander clusters (B1-4, HLA-DR-ADT$^+$/*UL123*^{low}), and one productively infected cluster (P, HLA-DR-ADT$^+$/*UL123*^{high}) (Fig. 1f, g).

moDCs comprise three transcriptionally defined cell subsets with different susceptibilities to infection

Cluster-specific marker gene expression profiles indicated that, for both donors, bystander clusters B1, B2 and B3 primarily originated from a single mock-exposed cluster, i.e., M1, M2, and M3, respectively (Fig. 2a,

b and Supplementary Fig. 2a). This was confirmed by canonical correlation analysis (CCA) predicting for each HCMV-NG exposed cell the most similar mock-exposed cells in an unbiased manner (Fig. 2c, d). The bystander cluster B1/2 from donor #1 originated from M1 and M2. Interestingly, bystander cells in cluster B4, and productively infected cells in P, were composed of cells from all three mock-exposed clusters. Importantly, M1-derived cells were the most abundant ones in cluster P (Fig. 2c, d), even after normalizing for the different cluster sizes of M1-M3 (Supplementary Fig. 2b, c).

Comparing cells from both donors using CCA revealed strong similarities between M1, M2 and M3, respectively (Fig. 2e), which similarly applied for their respective HCMV-NG exposed counterparts (Supplementary Fig. 2d). To address whether moDC clusters represented distinct subsets or different stages of differentiation, we performed RNA velocity analysis that predicts the upcoming gene expression of cells [19]. This analysis did not reveal any particular directionality among the clusters M1-3 (Fig. 2f). Instead, pathway analysis of moDC-specific traits revealed that the clusters M1-3 showed differences in metabolic pathways, cytokine production, endocytosis and in their antigen presentation capacity (Fig. 2g, Supplementary Fig. 2e and Supplementary Table 1). Notably, the respective clusters from donors #1 and #2 showed overall very similar profiles of active pathways. Taken together, moDCs comprise three distinct clusters that were similarly detected amongst mock- and HCMV-NG exposed moDCs derived from two independent donors.

Next, we verified via flow cytometry that mock-exposed moDCs showed a similar protein expression profile as detected in the moDC clusters using cluster-specific genes that were manually selected from the scRNA-seq data set, i.e., *CLEC12A* (CD371), *CD1a, CD86, CCL18, CCL17, CCL22*, *CSF1R* (CD115), *C5AR1* (CD88), and *LILRB2* (CD85d) (Fig. 3a-d and Supplementary Fig. 3a, b). In particular expression of CD1a, CD86 and CLEC12A distinguished the 3 subsets (Fig. 3b). M1 was characterized by $CD1a^-/CD86^-$, while showing high expression of CLEC12A. $CD1a^+$ defined M2 and $CD86^+$ defined M3. Analysis of moDCs from sixteen different donors verified the presence of these three subsets and indicated that $CD1a^-/CD86^-$ cells represented approximately 57%, $CD1a^+$ 28%, and $CD86^+$ 13% of moDCs (Fig. 3c). Furthermore, these markers discriminated the three subsets also in HCMV-NG exposed moDCs (Fig. 3e) and revealed higher percentages of NG^+ cells amongst $CD1a^-/CD86^-$ cells (M1) than amongst $CD86^+$ (M3) and $CD1a^+$ cells (M2) (Fig. 3f), consistent with our scRNA-seq data. Upon sorting, the three moDC subsets showed distinct morphologies (Fig. 3g). After HCMV-NG exposure the sorted $CD1a^-/CD86^-$ subset (M1) again showed higher infection than $CD1a^+$ cells (M2) (Fig. 3h). Only the sorted $CD86^+$ cells (M3) showed a higher susceptibility to infection than in the mixed moDC cultures, which was similar to $CD1a^-/CD86^-$ cells. Thus, flow cytometry validated the three moDC subsets with different susceptibilities to HCMV infection as identified by scRNA-seq.

Most HCMV-NG exposed moDCs contain virion-associated transcripts, but only few show *de novo* viral gene expression

Multiple HCMV genes commonly share a polyadenylation site. As 3' sequencing-based scRNA-seq cannot distinguish those, we manually curated groups of viral transcripts belonging to one polyadenylation site (Supplementary Fig. 4a). Analysis of viral transcripts revealed that most HCMV-NG exposed moDCs contained at least trace amounts of viral transcripts (Fig. 4a and Supplementary Fig. 1d). To distinguish virion-associated RNAs that were delivered to cells by the infection process and viral RNAs that were *de novo* transcribed, we sequenced the two HCMV-NG preparations V1 and V2 that were used for the infection experiments. In addition to viral transcripts, several thousands of different host transcripts were detected in HCMV-NG preparations (Fig. 4b). The four most abundant host transcripts included the heavy and light subunit of iron storage protein ferritin (*FTL, FTH1*) and the two polyubiquitin genes *UBB* and *UBC* (Fig. 4b). Moreover, we confirmed the late (L) viral transcript *UL22A* and the early (E) long non-coding *RNA2.7* as the most abundant virion-associated transcripts (Fig. 4b, c) [20]. Indeed, these transcripts were also the most abundant ones in bystander cells (Fig. 4d and Supplementary Fig. 4b). In contrast, productively infected cells in P showed promiscuous expression of viral transcripts of all kinetics classes. Interestingly, already at 8 hpi we found expression of E (e.g., *US22*) and L (e.g., *UL100*) transcripts in certain cells in P (Fig. 4e), which correlated with higher loads of total viral RNAs (Fig. 4a) as well as the virion-associated RNAs *UL22A* and *RNA2.7* (Supplementary Fig. 4c). To estimate for each cluster the percentage of cells that carried virion-associated RNAs as compared to the percentage of cells that started *de novo* viral gene expression, we analyzed the abundance of *UL22A/RNA2.7* versus *UL122/UL123* as prototypic virion-associated and *de novo* expressed RNAs, respectively. This analysis confirmed that close to 100% of cells in P were infected and started viral gene expression (Fig. 4f). Interestingly, up to 70% of the bystander cells in B1-3 had detectable levels of virion-associated transcripts *UL22A* and *RNA2.7* (Fig. 4f, left panel). Some variation of values was detected between clusters and donors and percentages were presumably underestimated due to RNA degradation during the 8 h of infection. In contrast, only 5-10% of cells in B1-3 and 25% of cells in B4 showed expression of *UL122* and *UL123* (Fig. 4f, right panel). Since percentages of NG^+ cells further increased between 8 and 24 h of incubation (Fig. 1a and Supplementary Fig. 1a) and the relative number of cells in P correlated with NG^+ cells at 8 hpi (Supplementary Fig. 1a, b), it is very likely that with time at least some of the bystander cells that showed UL122/UL123 expression would have progressed to productive infection. Cells in B4 expressed considerably higher levels of IE genes than cells in the other B clusters (Fig. 4d, f). Furthermore, in the UMAP, B4 was placed in close proximity to P (Fig. 1f, g). However, RNA velocity analysis did not reveal the transition of B4 to productively infected cells in P (Fig. 4g). Thus, upon HCMV-NG exposure, most moDCs are infected by virus particles that deliver viral and human RNAs into these cells, whereas *de novo* viral gene expression is initiated only in a minor fraction of moDCs.

Increased expression of viral RNAs is associated with downregulation of interferon stimulated genes and upregulation of heat shock proteins

Hallmark pathway analysis indicated that inflammatory pathways were significantly upregulated upon HCMV-NG exposure when compared with mock-exposed cells (Fig. 5a, first panel). Strikingly, inflammatory pathways were significantly downregulated in productively infected cells in P when

compared with bystander cells in B1-4 (Fig. 5a, second panel). Moreover, in bystander cells, mRNAs assigned to homeostatic/metabolic pathways were significantly negatively correlated with viral gene expression (Fig. 5a, third panel), whereas in productively infected cells mRNAs assigned to inflammatory and interferon response pathways were negatively correlated (Fig. 5a, fourth panel). Thus, downregulation of host response pathways to infection was qualitatively and quantitatively dependent on viral gene expression.

Interestingly, more host genes were downregulated (n=94) than upregulated (n=29) in productively infected cells (P) when compared with bystander cells (B) (Supplementary Table 2). Downregulated host genes were mostly negatively correlated with expression of viral RNAs and comprised predominantly ISGs (Fig. 5b). Indeed, we identified three ISGs as the most negatively correlated host genes in P, including (i) *IFI16* that was previously reported to be a restriction factor of early HCMV infection [21], (ii) *RNF213*, an ISG15 interactor [22]), and (iii) *TNFSF10* (TRAIL), the latter two of which so far have not been recognized to directly affect HCMV replication.

In contrast, in the few cases where host genes were upregulated in productively infected cells (P) they were mostly positively correlated with viral gene expression (Fig. 5b). This included the GTP-binding protein *RhoB* that was described earlier as a pro-viral factor for HCMV replication [23] and a broad range of heat shock proteins (HSPs) (Fig. 5b, c). In particular, the HSPs *DNAJB1* and *HSPA1A* were the host genes that were most positively correlated with viral RNA expression in P. Interestingly, also *IFNL1* (the gene encoding IFN-λ1) was one of the few host genes that was upregulated in P and that was positively correlated with viral gene expression. In contrast, *IFNB1* (the gene encoding IFN-β) was upregulated in P, but negatively correlated with viral gene expression (Fig. 5b). Thus, we identified putative pro- and anti-viral host factors of HCMV infection in moDCs.

Viral IE gene expression is correlated with *IFNB1* expression, whereas progression of viral infection inhibits *IFNB1*, but not *IFNL1* induction

We exposed moDCs to replication competent HCMV-NG and UV-inactivated HCMV-NG and analyzed cell free supernatants for the presence of IFN-α, IFN-β and IFN-λ. Both IFN-β and IFN-λ were mostly secreted within the first 16 hpi, whereas IFN-α secretion started later (Fig. 6a and Supplementary Fig. 5). Accordingly, mainly *IFNB1* and *IFNL1* expression was detected in the scRNA-seq analysis at 8 hpi. *IFNB1* was expressed in some cells of B1-3, B4 and P (Fig. 6b), whereas *IFNL1* expression was restricted mainly to B4 and some cells in P (Fig. 6c). In bystander cells, including B1-3 and B4, the expression of *IFNB1* and *IFNL1* positively correlated with levels of total viral RNAs (Fig. 6d). While *IFNL1* expression was also positively correlated with total viral RNA levels in P, *IFNB1* was negatively correlated suggesting a different mechanism of regulation for *IFNB1* and *IFNL1*. Therefore, we performed a detailed correlation of viral and host genes with *IFNB1* and *IFNL1* expression. In B1-B3 overall low correlations were detected (Fig. 6e, f and Supplementary Table 3, 4), including correlations with the most abundant viral RNAs in B1-B3, i.e., the virion-associated RNAs *UL22A/RNA2.7*. In contrast, the viral IE genes *UL122* and *UL123* showed a high correlation with *IFNB1*. In B4, *IFNB1* and *IFNL1* did not show a significant correlation with

most viral genes (Fig. 6e), whereas a large number of host genes was strongly correlated with both IFNs (Fig. 6f). In particular *PPP1R15A* (GADD34), which was found to mediate IFN-β expression under conditions of anti-viral protein synthesis inhibition in fibroblasts [24], was highly positively correlated with both IFNs in B4. *PPP1R15A* was also positively correlated with both IFNs in productively infected cells. However, the majority of strongly correlated host genes was either associated with *IFNB1* or *IFNL1* (Fig. 6f). This similarly applied to viral genes. *IFNB1* expression was only positively correlated with the viral IE gene *UL122*, while it was negatively correlated with all other viral RNAs (Fig. 6e). In stark contrast, in cells from P *IFNL1* was positively correlated with the majority of viral RNAs, and in particular with *UL22A* and *RNA2.7*. Thus, especially the host gene *PPP1R15A* seems to play an important role in the induction of both *IFNB1* and *IFNL1* in moDCs. Moreover, in bystander cells *IFNB1* expression was associated with viral IE gene transcription, whereas in P cells *IFNB1*, but not *IFNL1,* expression was counter-regulated upon progression of HCMV infection.

STING activation facilitates viral gene expression

To address the anti-viral activity of the different IFNs produced by HCMV-NG exposed moDCs, we treated moDCs with IFN-α2b, IFN-β or IFN-λ1 at the time of (0 dpi), or one day prior (-1 dpi) to HCMV-NG exposure. Treatment of moDCs with cytokines at the time of infection did not change the percentage of HCMV-NG$^+$ cells when compared with infected cells without treatment (Fig. 6g). In contrast, pre-treatment one day prior to HCMV-NG exposure with IFN-α2b and IFN-β, but not IFN-λ1, significantly reduced the percentage of NG positive cells indicating the anti-viral effect of IFN-α and IFN-β, but not IFN-λ1 under such conditions.

cGAS/STING recognition of HCMV DNA leads to activation of type I IFN expression in moDCs [10]. Since STING also activates NF-κB signaling [25] and NF-κB transactivates the HCMV major IE promoter [26,27], we hypothesized that cGAS/STING sensing of HCMV activated IE gene transcription, thus correlating *IFNB1* and *UL122/UL123* expression (Fig. 6e). While pre-treatment with the STING agonist ADU-S100 decreased susceptibility of moDCs to HCMV-NG infection presumably due to STING-mediated IFN induction, treatment at the time of infection significantly increased percentages of HCMV-NG$^+$ moDCs (Fig. 6h). Treatment with TNF-α that activates NF-κB similarly increased HCMV-NG infection suggesting that STING-dependent activation of IE gene expression was mediated by NF-κB.

moDCs reveal a marked downregulation of ISGs upon progression to productive infection

Commonly employed analysis pipelines for scRNA-seq data only consider reads originating from mature RNAs (“spliced reads”). As splicing occurs predominantly co-transcriptionally, the abundance of unspliced reads is a good approximation of nascent RNA that is currently being transcribed in an individual cell [19]. All HCMV-NG exposed moDCs, including cells in P, showed higher levels of spliced reads from ISGs than mock-exposed cells (Fig. 7a, left UMAP) suggesting that ISGs were initially induced also in productively infected cells. In contrast, unspliced reads for ISG transcripts were massively reduced in productively infected cells of P (Fig. 7a, right UMAP). Accordingly, the ratio of unspliced vs spliced ISG reads was

substantially lower in P than in B1-4 (Fig. 7b) suggesting downregulation of ISG transcription. A separate analysis of unspliced versus spliced transcripts in M1-3, B1-3, B4 and P confirmed that although all moDCs were competent to express ISGs upon HCMV-NG exposure, cells that contained intermediate amounts of viral RNA such as B4 moderately downregulated ISG transcription, and cells with strong viral gene expression in P showed massive downregulation of ISG transcription (Fig. 7c and Supplementary Fig. 6a-c). Notably, a subset of ISGs, including *ZC3HAV1* (ZAP) and *OASL*, were only strongly induced in B4 and P, but not in B1-3, and while their expression in P was inhibited this was not the case in B4 (Supplementary Fig. 6d, e). In P the extent of ISG shut off correlated with overall levels of viral gene expression (Fig. 7d, e). Interestingly, active ISG transcription was positively correlated with *UL122*, but negatively correlated with all other viral transcripts, in particular UL144-UL145, RNA2.7 and UL22A (Fig. 7f). These correlations indicated that massive suppression of ISG expression was initiated after the IE phase of viral infection.

Discussion

Analysis of scRNA-seq data from HCMV-NG exposed moDCs and validation of key findings on the protein level revealed a highly intricate relationship between HCMV gene expression, IFN induction and ISG expression that determines the outcome of HCMV infection of moDCs. We provide evidence that moDCs are composed of three distinct subsets, which support virus infection to different extents. We propose the following model: Upon virus encounter, the majority of moDCs gets infected by the virus. Predominantly cells that are infected by a high number of virus particles sense HCMV via the cGAS/STING axis, which leads to induction of IFN and STING-mediated activation of viral IE gene expression. IFN signaling then induces the expression of ISGs in all cells. In some cells where viral gene expression has started, high expression of specific ISGs suppresses the progression to productive infection and augments the induction of IFNs. However, in the majority of cells that show strong viral IE gene expression, viral infection progresses and viral immune evasion molecules efficiently inhibit ISG and *IFNB1*, but not *IFNL1*, expression.

As moDCs are extensively used in research as well as in clinical settings [28], it is necessary to understand the composition of moDC cultures. A recent paper analyzing scRNA-seq data of moDCs differentiated from a single donor in BSA-containing medium reported the presence of seven different subsets in moDCs [29]. Here we differentiated monocytes under serum-free conditions from two donors. This enabled us to minimize experimental variations and to integrate donor-associated variations. We only detected three transcriptionally distinct clusters, which were defined by characteristic surface markers: Subset 1 which is $CD1a^-/CD86^-/CLEC12A^+$, subset 2 which is $CD1a^+$, and subset 3 which is $CD86^+$. We verified the presence of these three subsets in moDCs derived from sixteen independent donors. Thus we confirmed earlier studies showing the existence of $CD1a^+$ and $CD1a^-$ moDCs [30,31] and additionally identified a third subset characterized by the expression of CD86. Interestingly, $CD1a^-/CD86^-/CLEC12A^+$ moDC supported viral gene expression to a larger extent than the other two subsets. Moreover, $CD1a^-/CD86^-/CLEC12A^+$ moDCs appeared to be the least suited subset for antigen presentation and showed high expression of

the tolerogenic chemokine CCL18 [32,33]. It is tempting to speculate that increased infection of tolerogenic DCs is a mechanism deployed by HCMV to induce regulatory T cells facilitating lytic and latent infection [34,35].

Previously, HCMV virions were shown to contain certain viral and host transcripts [11,20]. Analysis of the two HCMV-NG preparations used in this study revealed a plethora of previously undescribed virion-associated host transcripts. Some of these are highly upregulated at late times of infection and may thus promote productive infection upon delivery to newly infected cells. Particularly, the highly abundant heavy (*FTH*) and light chain (*FTL*) of the iron storage molecule ferritin might have functions in newly infected cells as HCMV replication and the typical “cytomegaly” phenotype of infected cells depend on iron [36]. Similarly, the two polyubiquitin gene transcripts *UBB* and *UBC* might be advantageous for the virus because HCMV repeatedly exploits and repurposes the ubiquitin proteasome system [37]. HCMV-encoded *RNA2.7* and *UL22A* are reported as the most abundant transcripts in late lytic and latent infection as well as the most abundant virion-associated transcripts [38,39]. We confirmed the latter and thus used the presence of *RNA2.7* and *UL22A* in moDCs as markers for viral entry. Since most HCMV-NG exposed moDCs contained these viral RNAs, we concluded that the majority of moDCs were infected by HCMV, whereas only a few cells supported the initiation of viral gene expression. Cells that did not support productive infection presumably were abortively infected. However, it is tempting to speculate that at least a fraction of these represent latently infected cells [39]. Conversely, the fact that only some of the infected cells started viral gene expression suggests that the onset of productive infection in moDCs is not critically defined by the viral entry, but rather by downstream events in the infected cell.

Studies in fibroblasts showed that the onset and progression of viral infection is dependent on the dose of infection per cell [15,40]. We found that already by 8 hpi, HCMV-NG exposed moDCs reached different stages of the virus life cycle, with some cells showing very promiscuous viral gene expression. As such cells also showed the highest level of virion-associated *UL22A* and *RNA2.7*, it is likely that also in our system a faster progression towards virus replication was caused by higher numbers of infecting virions per cell.

We found several host genes that were strongly correlated with viral RNA expression and might represent pro- and anti-viral factors that govern infection outcome. Among such host transcripts, we identified *RHOB*, which was described earlier as pro-viral during HCMV infection of fibroblasts [23], suggesting its relevance also for HCMV replication in moDCs. Other potential pro-viral genes were mainly HSPs. Several HSPs are already known to facilitate replication of herpesviruses including HCMV [41–43] and thus it is well possible that in particular *DNAJB1* and *HSPA1A* are pro-viral factors in HCMV infected moDCs. Conversely, among potential anti-viral factors, we found *IFI16*, which was previously characterized as anti-viral in immediate early and pro-viral in later stages of HCMV infection [21]. Other anti-viral candidates not described yet in the context of HCMV infected moDCs included the broadly anti-viral ISG15 interactor *RNF213* [22] and *TNFSF10* encoding the NK cell-activating protein TRAIL [44,45]. Since NK cells critically contribute to anti-HCMV immunity and HCMV-encoded *UL141* is known to block TRAIL receptors [46], the

particularly strong downregulation of TRAIL expression early upon infection that we observed here is likely another mechanism to escape NK cell-mediated killing.

The IFN response is critical for controlling HCMV infection. In accordance with some of our earlier studies, we found that not only productively infected but also bystander cells showed interferon production [10] and infection seemed to be a prerequisite for IFN induction in moDCs [47]. Interestingly, *IFNB1* expression was highly associated with *de novo* expression of *UL122/UL123*, although both viral genes have been reported to inhibit IFN-β induction [48]. Our data suggest that in moDCs that sense HCMV via the cGAS/STING pathway to induce *IFNB1* responses, STING additionally activates HCMV IE gene expression. This is presumably due to STING-dependent NF-κB activation [25] transactivating the major IE promoter [26,27]. This is consistent with similar findings in the murine cytomegalovirus model upon TLR stimulation [49]. Additionally, STING-mediated nuclear import of the viral genome [50] might enhance infection. Accordingly, we found that HCMV-NG infection and simultaneous STING activation significantly increased the percentage of infected moDCs verifying that HCMV is able to utilize one of the host's most early and central anti-viral responses to start its own replication.

We found that *IFNB1* was only expressed in cells that were still in the IE stage of viral gene expression, whereas its expression was inhibited upon progression of viral infection. In contrast, *IFNL1* expression was not inhibited by HCMV infection and was instead positively correlated with viral gene expression. Most of the known HCMV-encoded inhibitors of IFN expression such as *UL42* and *UL31* [51,52] do not target IFN-β directly, but molecules of the cGAS/STING sensing pathway, suggesting that *IFNB1* and *IFNL1* are induced differently in moDCs.

Productive infection rapidly shuts off ISG expression. Remarkably, by analyzing spliced and unspliced ISG transcripts, we found that the productively infected cells initially had expressed ISGs, which might even have facilitated HCMV infection, as proposed earlier [16]. Interestingly, among the viral transcripts that showed the highest association with the ISG shut off upon progression of infection, we found UL144-UL145. UL145 was recently identified to be essential for the induction of proteasomal degradation of STAT2 in fibroblasts [9]. Together with our data this suggests that UL145 is one of the major factors conferring efficient ISG shut off in moDCs.

As ISG expression was found to be highly heterogeneous in single cells [40], the outcome of infection might depend on the quality, quantity and kinetics of the set of induced ISGs. Indeed, we found strong similarities in host gene expression between clusters P and B4. However, while cells in P progressed towards productive infection, HCMV infection seemed to be abrogated in B4 after the IE stage. Specific ISGs such as *ZC3HAV1* (ZAP) and *OASL* were highly induced in cells of B4. ZAP has recently been shown to have high anti-HCMV potential [53] suggesting that these ISGs might facilitate inhibition of HCMV gene expression in B4. Abrogated HCMV infection might then allow for strong *IFNB1* expression, which is normally inhibited upon progression of viral infection. Accordingly, we found that B4 showed a particularly high abundance of *IFNB1* and *IFNL1* expressing cells.

In conclusion, scRNA-seq analysis of HCMV-NG exposed moDCs reveals complex interactions between the host cell and HCMV and unravels a dynamic interplay of seemingly contrasting functions such as induction of anti-viral responses as well as the support of productive infection.

Methods

Primary cell isolation and *in vitro* differentiation of monocyte-derived dendritic cells

Blood samples of healthy donors were obtained from the Blutspendedienst NSTOB (Niedersachsen-Sachsen-Anhalt-Thüringen-Oldenburg-Bremen gGmbH, Institut Springe) and the Institute for Transfusion Medicine and Transplant Engineering, Hannover Medical School, Germany (this work was approved by the ethics committee of the Hannover Medical School, ethical approval no. 8315_BO_K_2019). $CD14^+$ monocytes were isolated from PBMC by MACS sorting. For differentiation of monocyte-derived dendritic cells (moDCs), 5 x 10^5/ml of the monocytes were cultivated for 5 days in serum-free CellGenix® GMP DC medium (CellGenix) enriched with 1000 U/ml GM-CSF (granulocyte macrophage-colony stimulating factor, Miltenyi) and 1000 U/ml IL-4 (interleukin 4, Miltenyi).

Virus

The reporter TB40E virus strain containing an *UL122/123*-mNeonGreen tag (HCMV-NG) was described previously [17]. In brief, the NG gene was linked to the P2A peptide that was inserted before the start codon of the *UL122/123* exon. Virus was propagated in lung fibroblasts (MRC5- ATCC® CCL-171™). Virus was concentrated from cells and supernatant by centrifugation for 3h at 25,000 x g and additionally purified using 20% sorbitol gradient centrifugation at 53,000 x g, 10°C for 1 h 15 min. Infectious virus yields were assayed on MRC-5 cells as described previously [54].

Infection procedures

For infection of moDCs, the cells were either mock or HCMV-NG exposed at MOI 6. In some experiments HCMV-NG was UV inactivated using 999 mJ/cm^2 prior to moDC treatment. Infection was enhanced by centrifugation at 300g for 30 min. scRNA-Seq was performed at 8 hpi and flow cytometry analysis was performed at 8 hpi and 24 hpi.

Flow cytometry analysis and cell sorting

moDCs were harvested and labeled with Zombie Aqua™ Fixable Viability Kit (Biolegend). Surface marker immunolabeling was performed in cold flow cytometry buffer (PBS, BSA, EDTA) with the following antibodies: CD1a, CD85d, CD86, CD88, CD115 and CLEC12A (Biolegend). Immunolabeling of the cells was performed for 20 min at 4°C. Intracellular CCL17, CCL18 and CCL22 immunolabeling was performed according to the intracellular staining protocol from BD Bioscience. Then the samples were acquired on a SP6800 or ID7000 (Sony) and the data were analyzed using FlowJo software (Tree Star). RFI was

calculated as the ratio of the mean fluorescence intensity (MFI) of the antibody staining and the isotype staining.

For cell sorting moDCs were harvested on day 5 of differentiation, stained with Viobility™ Fixable Dyes (Miltenyi) and immunolabeled with anti-CD1a and anti-CD86 antibodies (Biolegend). Sorting of $CD1a^+$, $CD86^+$ and $CD1a^-/CD86^-$ cell subsets was performed using the MACSQuant® Tyto® sorter (Miltenyi). Afterwards cells were plated in fresh CellGenix® GMP DC medium (CellGenix) for 24 h and subsequently infected with HCMV-NG for 24 h.

ELISA analysis

Cell-free supernatants were analyzed using the Human IFN-alpha Platinum ELISA (Thermofisher), human IFN Beta and Lambda ELISA kit (PBL) according to the manufacturer's instructions.

In vitro treatment with cytokines and STING agonists

Treatment with 10 µM ADU-S100 (purchased from MedChem express), 1 ng/ml TNF-α (Miltenyi), 100 U/ml IFN-α2b (IntronA, MSD), 1 ng/ml IFN-β and 10 ng/ml IFN-λ1 (Peprotech) was performed 1 day (-1 dpi) before HCMV-NG exposure or at time of exposure (0 dpi) at 37°C. Subsequently, samples were harvested 1 day post HCMV-NG exposure as described above to determine NG^+ cell percentages by flow cytometry.

CITE-seq labeling, single cell library preparation and sequencing

moDCs from two healthy, HCMV seronegative, male donors were prepared and infected as described above. Afterwards, mock and HCMV-NG exposed cells were CITEseq labelled with TotalSeq^{TM}-B antibodies anti-human CD45 (anti-CD45-ADT, mock-exposed cells) or anti-human HLA-DR antibody (anti-HLA-DR-ADT, HCMV-NG exposed cells) (Biolegend) according to the manufacturer's protocol for TotalSeq^{TM}-B antibodies with 10X 3' Reagent Kit v3.0 Feature Barcoding Technology.

In brief, $1x10^6$ mock and HCMV-NG exposed cells from each of the four groups ($1x10^6$ cells/ml) were resuspended separately in 50 µl Cell Staining Buffer (BioLegend). Subsequently, 5 µl of Human TruStain FcX™ Fc Blocking reagent (BioLegend) were added and incubated for 10 min at 4°C. After the incubation 1 µg anti-human CD45 or anti-human HLA-DR TotalSeq-B antibody were added to the cell suspension and incubated for 30 minutes at 4°C.

The cells were washed in 1.5 ml staining buffer and centrifuged for 5 minutes at 400 x g and 4°C.

Subsequently, the cells were resuspended in an appropriate volume of 1x DPBS (Gibco), passed through a 40 µm mesh (FlowmiTM Cell Strainer, Merck) and counted, using a Neubauer counting chamber (Marienfeld). 1/3 of mock cells was pooled with 2/3 of HCMV-NG exposed cells. Importantly, mock-exposed cells that were derived from the same sample were combined with HCMV-NG V1 and V2 exposed cells to provide an internal control for batch effects.

Labeled cell suspensions were loaded in the Chromium™ Controller (10x genomics). Single Cell 3' reagent kit v3.1 was used for reverse transcription, cDNA amplification and library construction following the detailed protocol provided by 10x Genomics. CITE-seq libraries were prepared according to the Feature barcoding protocol for 10x Single Cell 3' Reagent Kit v3.

SimpliAmp Thermal Cycler was used for amplification and incubation steps (Applied Biosystems). Libraries were quantified by Qubit™ 3.0 Fluometer (ThermoFisher) and quality was checked using 2100 Bioanalyzer with High Sensitivity DNA kit (Agilent). Sequencing was performed in paired-end mode with S2 2 × 50 cycles kit using NovaSeq 6000 sequencer (Illumina).

Sequencing of virus preparations

To analyze the virion-associated RNA within the employed virus preparations, RNA was extracted from $1.3x10^8$ plaque forming units per ml of virus stock with the Quick-RNA Viral kit (Zymo) by using 10 µl from 2 independent viral preparations (V 1 and V 2). RNA was eluted in 6 µl nuclease-free water and 3 µl were used for the Smart-seq v4 low input reaction (Takara) with one-quarter of the recommended reagent volumes. ERCC spike-in control was added to a dilution of 1:20 millions. Libraries were prepared using Nextera XT (Illumina) using a quarter of the recommended reagent volumes, pooled and sequenced in paired-end mode on the NextSeq 500 sequencer (Illumina) using the Mid Output 2×75 cycle kit.

Single cell read mapping and counting

We used the 10x Genomics CellRanger software (version 3.0.2) to map the "Gene expression" libraries against a combined index of the human (HG38, Ensembl v90 annotations; filtered to include only "protein_coding", "lincRNA", "antisense", "IG" and "TR" genes, as recommended in the CellRanger documentation) and HCMV (GenBank accession: EF999921), which was adapted to include the NeonGreen cassette in the viral genome. The TotalSeq-B antibody libraries were mapped against the CellRanger internal index. Using an in-house genome browser, we then went through the viral genome and manually annotated significant clusters of reads at polyadenylation sites (Supplementary Fig. 4a). We created a new combined index of human (see above) and these new annotations of read clusters as a replacement of the annotated viral open reading frames and ran CellRanger again to obtain the final expression matrices. Overall, this resulted in 26,395 cells after the default filtering from CellRanger.

Processing of Smart-seq data from virus preparations

Smart-seq data from the two virus preparations were mapped against the combined index generated by CellRanger using STAR (version 2.5.3a) [55] with standard parameters. Since these data contained reads not only from the 3' ends of mRNAs, we adapted the cluster annotations for read counting as follows. We identified the closest cluster upstream of each cluster to define the upstream distance. If this was greater than 1,000 nt, we set it to 1,000. Then, each cluster was extended in the upstream direction by its upstream distance. We manually compared these annotations with the observed read coverages in a genome browser to confirm these manual annotations.

Demultiplexing, quality control and preprocessing of 10x scRNA-seq data

Centered log-ratio normalization was applied to the TotalSeq counts and strict thresholds for demultiplexing were identified in a scatterplot of the CD45-ADT value vs. the HLA-DR-ADT value. We decided to call all cells with HLA-DR-ADT value > 0.35 as HCMV-NG exposed, and all cells with CD45-ADT value >0.9 as mock. Double negative cells (n=1,151) and doublets (n=869) were removed. We further removed all cells with less than 10,000 or more than 40,000 detected UMIs and with more than 17% mitochondrial RNA, which left us with 13,566 HCMV-NG exposed and 5,270 mock cells.

We then used the SCTransform pipeline to normalize the remaining cells [56] and performed principal component analysis. Based on elbow plot analysis we used the first 45 principal components to compute the shared nearest neighbor graph and performed Louvain clustering (resolution 0.8) [57]. The UMAP algorithm [58] was run on the first 45 principal components with standard parameters. A second UMAP was computed by the same procedure after first removing viral genes from the expression matrix.

Two clusters were identified to be composed of doublets and were removed. Clusters 3 in CD45-ADT$^+$ cells and clusters 8 and 9 in HLA-DR-ADT$^+$ cells (see Fig. 1c-d) were clusters composed of cells from both donors and were split according to donor origin. For all other clusters one donor was dominant (>95% of all cells), and cells from the other donor were removed.

Integration analyses

We used canonical correlation analysis as described [59] and implemented in Seurat (IntegrateData function) to integrate defined subsets of cells in our data with other subsets. In each case, we removed all viral genes from the integration features.

To integrate the mock-exposed cells, we first removed all “B” and “P” clusters and split the remaining cells according to donor information. The integration of bystander and productively infected cells with the mock-exposed cells were performed for each donor separately. To compute the composition of bystander and productively infected cells according to their corresponding cluster in the mock-exposed cells, we computed the k nearest neighbor graph (with k set to 5% of all cells used) for the integrated data set. Each bystander or productively infected cell was then assigned to a mock-exposed cluster based on a majority vote among the nearest neighbors.

RNA velocity and ISG unspliced vs. spliced analysis

We first ran the run10x command from the velocyto package [19] to extract count matrices for spliced and unspliced reads from the bam files generated by CellRanger. RNA velocities were then computed using the velocyto R package with kCells set to 15, and the velocity plot was generated by calling the show.velocity.on.embedding.cor function on the UMAP computed by CellRanger.

To compute the unspliced over spliced ratio for ISGs, we first computed the 20 nearest neighbors for each cell and then computed the convolution for both spliced and un-spliced count matrices by matrix multiplication of the adjacency matrix of the nearest neighbor graph. The total spliced or un-spliced value for each cell was then computed as the total sum of all HALLMARK_INTERFERON_ALPHA_RESPONSE genes from MSigDB.

Pathway enrichment

For pathway analysis, we first computed marker genes for each donor separately using the fast Wilcoxon test (wilcoxauc function from the presto package). We then ran the gsva function from the GSVA R package using the average expression values per cluster on a predefined set of pathways. All selected pathways were chosen from MSigDB and can be found in Fig. 2g, Supplementary Fig. 2e and Supplementary Table 1.

Correlation and fold change analysis

To compute fold changes between HCMV-NG and mock-exposed cells we extracted the averages per cluster from the SCTransform-normalized data. We then computed the log2 fold change of the average over all mock-exposed over the bystander clusters. The fold changes of productively infected cells over bystander cells were computed using the wilcoxauc function from the presto package. Spearman correlations with the total percentage of viral gene expression for each gene were computed using the base cor R function. The gene set enrichment test was computed using a two-sided Wilcoxon test comparing the fold changes or correlation coefficients from genes that belong to a particular gene set against genes not belonging to the gene set. Only the highly variable genes defined by SCTransform and all gene sets from the Hallmark category of MSigDB [60] were considered (Supplementary Table 2).

The Spearman correlations of viral or cellular genes with *IFNB1* or *IFNL1* expression (Supplementary Table 3, 4) or the ISG inhibition value (unspliced over spliced RNA) were computed using base cor R function using the cells from the productively infected cluster only.

Data and software availability

scRNA-seq data generated during this study are in the process of being deposited at the European Genome-phenome Archive (EGA), which is hosted by the EBI and the CRG. Data can be browsed via the interface: einstein.virologie.uni-wuerzburg.de:3839/45559dc12750521deffaff3b105e9615/

References

1. Organization, W. H., Control, C. f. D. & Prevention. Birth defects surveillance: a manual for programme managers. (2020).
2. Taylor-Wiedeman, J., Sissons, J. G., Borysiewicz, L. K. & Sinclair, J. H. Monocytes are a major site of persistence of human cytomegalovirus in peripheral blood mononuclear cells. *J Gen Virol* **72** (**Pt 9**),

2059–2064, doi:10.1099/0022-1317-72-9-2059 (1991).

3. Sinzger, C., Plachter, B., Grefte, A., The, T. H. & Jahn, G. Tissue macrophages are infected by human cytomegalovirus in vivo. *J Infect Dis* **173**, 240–245, doi:10.1093/infdis/173.1.240 (1996).
4. Spector, W. G., Walters, M. N. & Willoughby, D. A. The origin of the mononuclear cells in inflammatory exudates induced by fibrinogen. *J Pathol Bacteriol* **90**, 181–192, doi:10.1002/path.1700900119 (1965).
5. Shi, C. & Pamer, E. G. Monocyte recruitment during infection and inflammation. *Nat Rev Immunol* **11**, 762–774, doi:10.1038/nri3070 (2011).
6. Brinkmann, M. M. *et al.* Cytomegalovirus immune evasion of myeloid lineage cells. *Med Microbiol Immunol* **204**, 367–382, doi:10.1007/s00430-015-0403-4 (2015).
7. Sinclair, J. Manipulation of dendritic cell functions by human cytomegalovirus. *Expert Rev Mol Med* **10**, e35, doi:10.1017/S1462399408000872 (2008).
8. Goodwin, C. M., Ciesla, J. H. & Munger, J. Who's Driving? Human Cytomegalovirus, Interferon, and NFκB Signaling. *Viruses* **10**, doi:10.3390/v10090447 (2018).
9. Le-Trilling, V. T. K. *et al.* The Human Cytomegalovirus pUL145 Isoforms Act as Viral DDB1-Cullin-Associated Factors to Instruct Host Protein Degradation to Impede Innate Immunity. *Cell Rep* **30**, 2248-2260 e2245, doi:10.1016/j.celrep.2020.01.070 (2020).
10. Paijo, J. *et al.* cGAS Senses Human Cytomegalovirus and Induces Type I Interferon Responses in Human Monocyte-Derived Cells. *PLoS Pathog* **12**, e1005546, doi:10.1371/journal.ppat.1005546 (2016).
11. Bresnahan, W. A. & Shenk, T. A subset of viral transcripts packaged within human cytomegalovirus particles. *Science* **288**, 2373–2376, doi:10.1126/science.288.5475.2373 (2000).
12. Varnum, S. M. *et al.* Identification of proteins in human cytomegalovirus (HCMV) particles: the HCMV proteome. *J Virol* **78**, 10960–10966, doi:10.1128/JVI.78.20.10960-10966.2004 (2004).
13. Stinski, M. F. Human cytomegalovirus: glycoproteins associated with virions and dense bodies. *J Virol* **19**, 594–609, doi:10.1128/JVI.19.2.594-609.1976 (1976).
14. Fortunato, E. A. Use of diploid human fibroblasts as a model system to culture, grow, and study human cytomegalovirus infection. *Methods Mol Biol* **1119**, 47–57, doi:10.1007/978-1-62703-788-4_4 (2014).
15. Hein, M. Y. & Weissman, J. S. Functional single-cell genomics of human cytomegalovirus infection. *bioRxiv*, doi:10.1101/775080 (2021).
16. Galinato, M. *et al.* Single-Cell Transcriptome Analysis of CD34(+) Stem Cell-Derived Myeloid Cells Infected With Human Cytomegalovirus. *Front Microbiol* **10**, 577, doi:10.3389/fmicb.2019.00577 (2019).
17. Kasmapour, B. *et al.* Myeloid Dendritic Cells Repress Human Cytomegalovirus Gene Expression and Spread by Releasing Interferon-Unrelated Soluble Antiviral Factors. *J Virol* **92**, doi:10.1128/JVI.01138-17 (2018).

18. Zheng, G. X. *et al.* Massively parallel digital transcriptional profiling of single cells. *Nat Commun* **8**, 14049, doi:10.1038/ncomms14049 (2017).
19. La Manno, G. *et al.* RNA velocity of single cells. *Nature* **560**, 494–498, doi:10.1038/s41586-018-0414-6 (2018).
20. Mohammad, A. A. *et al.* Human cytomegalovirus microRNAs are carried by virions and dense bodies and are delivered to target cells. *J Gen Virol* **98**, 1058–1072, doi:10.1099/jgv.0.000736 (2017).
21. Gariano, G. R. *et al.* The intracellular DNA sensor IFI16 gene acts as restriction factor for human cytomegalovirus replication. *PLoS Pathog* **8**, e1002498, doi:10.1371/journal.ppat.1002498 (2012).
22. Thery, F. *et al.* Ring Finger Protein 213 Assembles into a Sensor for ISGylated Proteins with Antimicrobial Activity. *bioRxiv*, doi: 10.1101/2021.06.03.446796 (2021).
23. Goulidaki, N. *et al.* RhoB is a component of the human cytomegalovirus assembly complex and is required for efficient viral production. *Cell Cycle* **14**, 2748–2763, doi:10.1080/15384101.2015.1066535 (2015).
24. Dalet, A. *et al.* Protein synthesis inhibition and GADD34 control IFN-beta heterogeneous expression in response to dsRNA. *EMBO J* **36**, 761–782, doi:10.15252/embj.201695000 (2017).
25. Abe, T. & Barber, G. N. Cytosolic-DNA-mediated, STING-dependent proinflammatory gene induction necessitates canonical NF-kappaB activation through TBK1. *J Virol* **88**, 5328–5341, doi:10.1128/JVI.00037-14 (2014).
26. DeMeritt, I. B., Milford, L. E. & Yurochko, A. D. Activation of the NF-kappaB pathway in human cytomegalovirus-infected cells is necessary for efficient transactivation of the major immediate-early promoter. *J Virol* **78**, 4498–4507, doi:10.1128/jvi.78.9.4498-4507.2004 (2004).
27. Sambucetti, L. C., Cherrington, J. M., Wilkinson, G. W. & Mocarski, E. S. NF-kappa B activation of the cytomegalovirus enhancer is mediated by a viral transactivator and by T cell stimulation. *Embo j* **8**, 4251–4258, doi: 10.1002/j.1460-2075.1989.tb08610.x (1989).
28. Davis, I. D., Jefford, M., Parente, P. & Cebon, J. Rational approaches to human cancer immunotherapy. *J Leukoc Biol* **73**, 3–29, doi:10.1189/jlb.0502261 (2003).
29. Gao, Y. *et al.* Single-Cell Analysis Reveals the Heterogeneity of Monocyte-Derived and Peripheral Type-2 Conventional Dendritic Cells. *J Immunol* **207**, 837–848, doi:10.4049/jimmunol.2100094 (2021).
30. Gogolak, P. *et al.* Differentiation of CD1a- and CD1a+ monocyte-derived dendritic cells is biased by lipid environment and PPARgamma. *Blood* **109**, 643–652, doi:10.1182/blood-2006-04-016840 (2007).
31. Majai, G. *et al.* PPARgamma modulated inflammatory response of human dendritic cell subsets to engulfed apoptotic neutrophils. *J Leukoc Biol* **88**, 981–991, doi:10.1189/jlb.0310144 (2010).
32. Azzaoui, I. *et al.* CCL18 differentiates dendritic cells in tolerogenic cells able to prime regulatory T cells in healthy subjects. *Blood* **118**, 3549–3558, doi:10.1182/blood-2011-02-338780 (2011).

33. Bellinghausen, I. *et al.* Enhanced production of CCL18 by tolerogenic dendritic cells is associated with inhibition of allergic airway reactivity. *J Allergy Clin Immunol* **130**, 1384–1393, doi:10.1016/j.jaci.2012.08.039 (2012).
34. Almanan, M. *et al.* Tissue-specific control of latent CMV reactivation by regulatory T cells. *PLoS Pathog* **13**, e1006507, doi:10.1371/journal.ppat.1006507 (2017).
35. Jost, N. H. *et al.* Regulatory T cells and T-cell-derived IL-10 interfere with effective anti-cytomegalovirus immune response. *Immunol Cell Biol* **92**, 860–871, doi:10.1038/icb.2014.62 (2014).
36. Crowe, W. E., Maglova, L. M., Ponka, P. & Russell, J. M. Human cytomegalovirus-induced host cell enlargement is iron dependent. *Am J Physiol Cell Physiol* **287**, C1023-1030, doi:10.1152/ajpcell.00511.2003 (2004).
37. Le-Trilling, V. T. K. & Trilling, M. Ub to no good: How cytomegaloviruses exploit the ubiquitin proteasome system. *Virus Res* **281**, 197938, doi:10.1016/j.virusres.2020.197938 (2020).
38. Rossetto, C. C., Tarrant-Elorza, M. & Pari, G. S. Cis and trans acting factors involved in human cytomegalovirus experimental and natural latent infection of CD14 (+) monocytes and CD34 (+) cells. *PLoS Pathog* **9**, e1003366, doi:10.1371/journal.ppat.1003366 (2013).
39. Shnayder, M. *et al.* Defining the Transcriptional Landscape during Cytomegalovirus Latency with Single-Cell RNA Sequencing. *mBio* **9**, doi:10.1128/mBio.00013-18 (2018).
40. Erhard, F. *et al.* scSLAM-seq reveals core features of transcription dynamics in single cells. *Nature* **571**, 419–423, doi:10.1038/s41586-019-1369-y (2019).
41. Russell, J., Stow, E. C., Stow, N. D. & Preston, C. M. Abnormal forms of the herpes simplex virus immediate early polypeptide Vmw175 induce the cellular stress response. *J Gen Virol* **68** (**Pt 9**), 2397–2406, doi:10.1099/0022-1317-68-9-2397 (1987).
42. Santomenna, L. D. & Colberg-Poley, A. M. Induction of cellular hsp70 expression by human cytomegalovirus. *J Virol* **64**, 2033–2040, doi:10.1128/JVI.64.5.2033-2040.1990 (1990).
43. Pei, Y. *et al.* A Hsp40 chaperone protein interacts with and modulates the cellular distribution of the primase protein of human cytomegalovirus. *PLoS Pathog* **8**, e1002968, doi:10.1371/journal.ppat.1002968 (2012).
44. Hymowitz, S. G. *et al.* Triggering cell death: the crystal structure of Apo2L/TRAIL in a complex with death receptor 5. *Mol Cell* **4**, 563–571, doi:10.1016/s1097-2765(00)80207-5 (1999).
45. Ramamurthy, V. *et al.* The structure of the death receptor 4-TNF-related apoptosis-inducing ligand (DR4-TRAIL) complex. *Acta Crystallogr F Struct Biol Commun* **71**, 1273–1281, doi:10.1107/S2053230X15016416 (2015).
46. Smith, W. *et al.* Human cytomegalovirus glycoprotein UL141 targets the TRAIL death receptors to thwart host innate antiviral defenses. *Cell Host Microbe* **13**, 324–335, doi:10.1016/j.chom.2013.02.003 (2013).
47. Becker, J. *et al.* Human monocyte-derived macrophages inhibit HCMV spread independent of classical antiviral cytokines. *Virulence* **9**, 1669–1684, doi:10.1080/21505594.2018.1535785 (2018).

48. Kim, J. E., Kim, Y. E., Stinski, M. F., Ahn, J. H. & Song, Y. J. Human Cytomegalovirus IE2 86 kDa Protein Induces STING Degradation and Inhibits cGAMP-Mediated IFN-beta Induction. *Front Microbiol* **8**, 1854, doi:10.3389/fmicb.2017.01854 (2017).
49. Kropp, K. A. *et al.* A temporal gate for viral enhancers to co-opt Toll-like-receptor transcriptional activation pathways upon acute infection. *PLoS Pathog* **11**, e1004737, doi:10.1371/journal.ppat.1004737 (2015).
50. Hong, Y. *et al.* STING facilitates nuclear import of herpesvirus genome during infection. *Proc Natl Acad Sci U S A* **118**, doi:10.1073/pnas.2108631118 (2021).
51. Huang, Z. F. *et al.* Human Cytomegalovirus Protein UL31 Inhibits DNA Sensing of cGAS to Mediate Immune Evasion. *Cell Host Microbe* **24**, 69-80 e64, doi:10.1016/j.chom.2018.05.007 (2018).
52. Fu, Y. Z. *et al.* Human cytomegalovirus protein UL42 antagonizes cGAS/MITA-mediated innate antiviral response. *PLoS Pathog* **15**, e1007691, doi:10.1371/journal.ppat.1007691 (2019).
53. Gonzalez-Perez, A. C. *et al.* The Zinc Finger Antiviral Protein ZAP Restricts Human Cytomegalovirus and Selectively Binds and Destabilizes Viral UL4/UL5 Transcripts. *mBio* **12**, doi:10.1128/mBio.02683-20 (2021).
54. Le, V. T. K., Trilling, M., Wilborn, M., Hengel, H. & Zimmermann, A. Human cytomegalovirus interferes with signal transducer and activator of transcription (STAT) 2 protein stability and tyrosine phosphorylation. *J Gen Virol* **89**, 2416–2426, doi:10.1099/vir.0.2008/001669-0 (2008).
55. Dobin, A. *et al.* STAR: ultrafast universal RNA-seq aligner. *Bioinformatics* **29**, 15–21, doi:10.1093/bioinformatics/bts635 (2013).
56. Hafemeister, C. & Satija, R. Normalization and variance stabilization of single-cell RNA-seq data using regularized negative binomial regression. *Genome Biol* **20**, 296, doi:10.1186/s13059-019-1874-1 (2019).
57. Blondel, V. D., Guillaume, J.-L., Lambiotte, R. & Lefebvre, E. Fast unfolding of communities in large networks. *J. Stat. Mech. Theory Exp.* **2008**, P10008, doi: 10.1088/1742-5468/2008/10/P10008 (2008).
58. McInnes, L., Healy, J. & Melville, J. Umap: Uniform manifold approximation and projection for dimension reduction. *arXiv preprint arXiv:1802.03426* (2018).
59. Stuart, T. *et al.* Comprehensive Integration of Single-Cell Data. *Cell* **177**, 1888-1902 e1821, doi:10.1016/j.cell.2019.05.031 (2019).
60. Subramanian, A. *et al.* Gene set enrichment analysis: a knowledge-based approach for interpreting genome-wide expression profiles. *Proc Natl Acad Sci U S A* **102**, 15545–15550, doi:10.1073/pnas.0506580102 (2005).

Declarations

Acknowledgements

We thank Olivia Luise Gern, Luise Krajewski and Zeinab Kanso for help with some experiments, and Elizabeth Janecek-Erfurth for help with the submission of the manuscript. We especially thank the Blutspendedienst NSTOB (Niedersachsen-Sachsen-Anhalt-Thüringen-Oldenburg-Bremen gGmbH, Institut Springe) for providing buffy coats. Graphics were created using BioRender. This study was supported by grants from the Bavarian Ministry of Economic Affairs and Media, Energy and Technology (grant allocation nos. 0703/68674/5/2017 and 0703/89374/3/2017; to L.D., A.-E.S., F.E. and U.K.), the German Research Foundation (DFG; Project ID 158989968 - SFB 900-B2 to L.C.-S. and U.K.; Project ID 398367752 – FOR 2830, to B.E.-V. and U.K.; Project ID ER 927/2-1 – FOR2830 to F.E., Project ID ER 927/1-1 to F.E.), the EU Marie Skłodowska-Curie Actions Innovative Training Network (VIROINF: 955974) to L.D and F.E., Ministry for Science and Culture of Lower Saxony (research consortium COALITION, to U.K.) and by the German Research Foundation (DFG) under Germany's Excellence Strategy (EXC 2155 "RESIST" – Project ID 39087428 to U.K).

Author contributions

Conceptualization, B.C., J.B., U.K.; Methodology, B.C. and J.B.; Software, B.C., F.M. and F.E.; Validation, B.C.; Formal Analysis, B.C., J.B. and F.E.; Investigation, B.C., J.B., T.K., A.P. and V.D.; Resources, F.M., F.E., L.C.-S., X.C., Y. L. and B.E.-V.; Data curation, F.M., F.E., X.C. and Y. L.; Writing-Original Draft, B.C., J.B., F.E. and U.K.; Writing- Review & Editing, A.E.S., A.P., L.C.S., T.K., Y.L., L.D. and B.E.V.; Visualization, B.C., J.B., F.E. and U.K.; Supervision, J.B. and U.K.; Funding Acquisition, L.C.S., F.E., U.K., A.E.S., L.D.

Declaration of interest

The authors declare no competing interests.

Figures

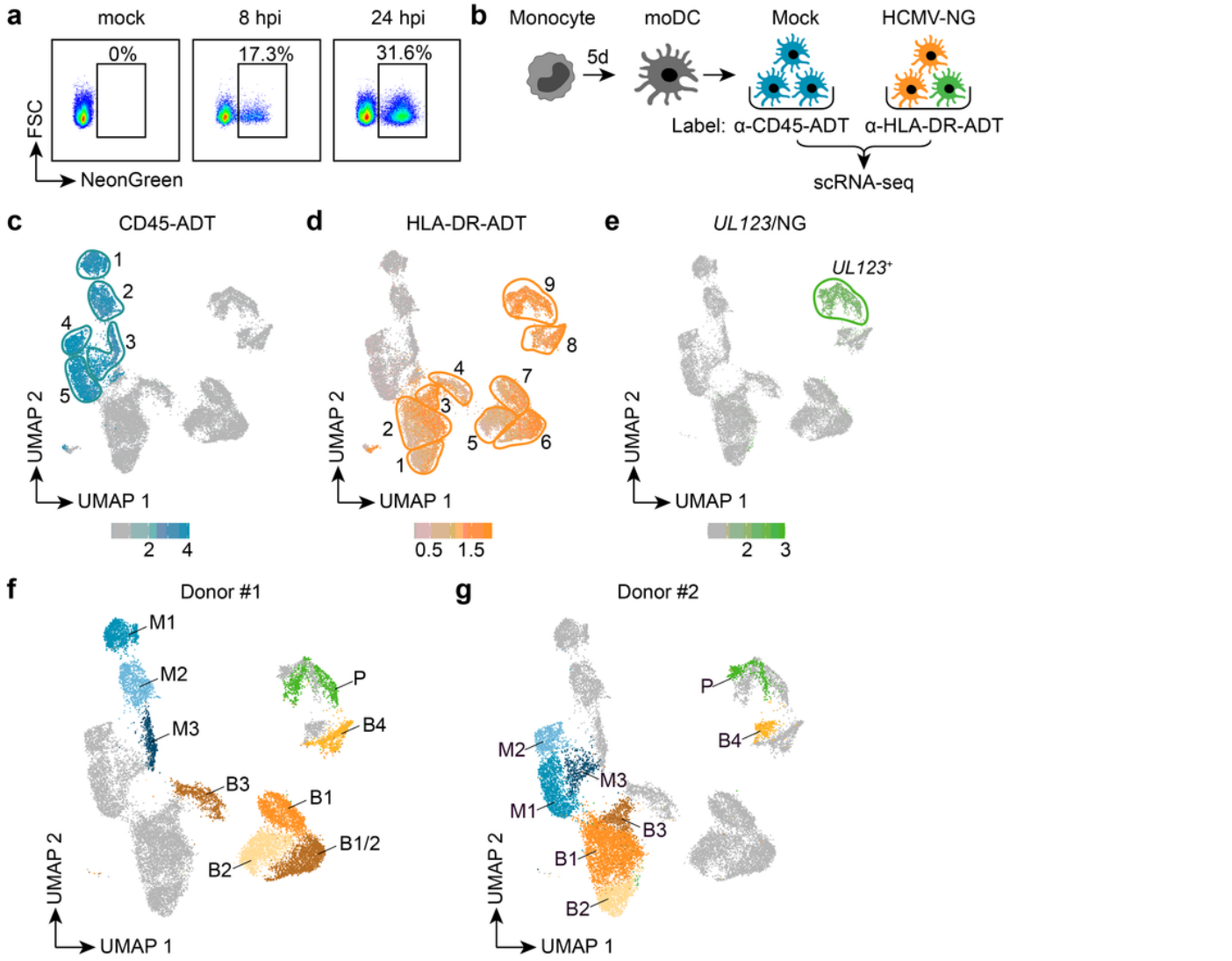

Fig. 1

Figure 1

Single-cell RNA sequencing reveals heterogeneity of human monocyte-derived dendritic cells. Blood-derived CD14^{+} monocytes were differentiated to moDCs and exposed with HCMV-NG (NeonGreen) at MOI 6. **a** Flow cytometry analysis of mock and HCMV-NG exposed moDCs 0, 8 and 24 hours post infection (hpi). **b** Schematic depiction of the experimental setup. Mock and HCMV-NG exposed moDCs were labeled with anti-CD45-ADT and anti-HLA-DR-ADT antibodies 8 hpi and pooled prior to scRNA-seq. This experiment was performed in four runs with moDCs from two donors and with two independent virus preparations. **c, d** Data from all four scRNA-seq runs were combined for non-linear dimensionality reduction (UMAP) and unsupervised clustering (bordered and numbered areas). Log normalized feature counts are shown for CD45-ADT (**c**) and HLA-DR-ADT (**d**). Two clusters were identified to be composed of doublets and were removed for further analysis. **e** SCTransform normalized feature counts for the viral *UL123*/*NeonGreen* fusion gene. **f** Donor #1 and **g** donor #2 comprised 3 mock-exposed clusters (M1-3, CD45-ADT^{+}), 4-5 bystander clusters (B1-4, HLA-DR-ADT^{+}/*UL123*^{low}), and 1 productively infected cluster (P, HLA-DR-ADT^{+}/*UL123*^{high}).

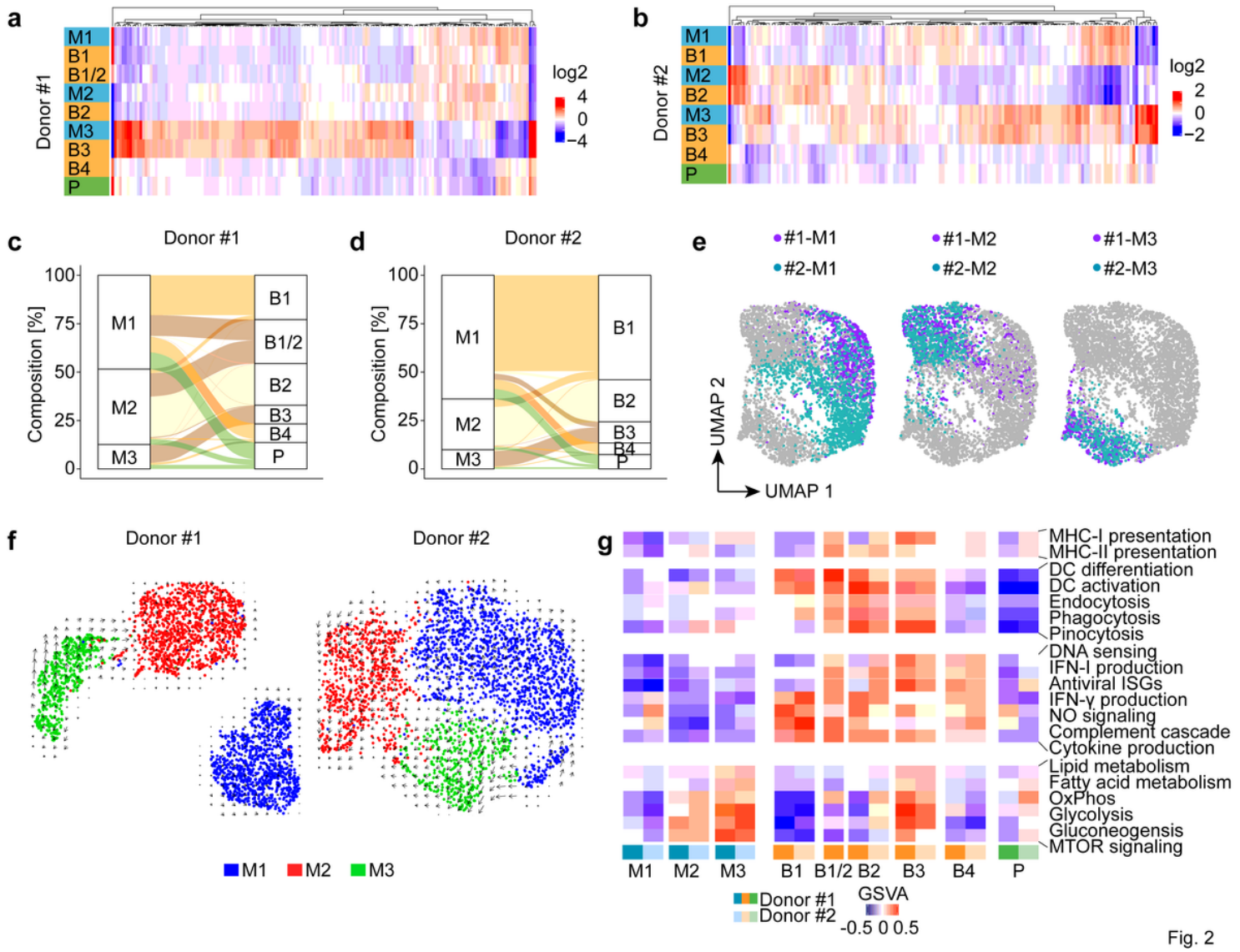

Figure 2

HCMV-NG exposed moDCs can be traced back to three distinct clusters identified in mock-exposed moDCs. a, b Heat map showing the average expression per cluster (log_2-fold change vs. the grand mean) of marker genes that were common in mock and HCMV-NG exposed cells of donor #1 (**a**) and donor #2 (**b**). **c, d** Alluvial charts showing the contribution of mock moDCs to HCMV-NG exposed clusters of donor #1 (**c**) and donor #2 (**d**). **e** Donor integration by canonical correlation analysis of M1, M2, and M3 clusters of each donor highlighted in separate UMAPs. **f** UMAP embedding of M1, M2 and M3 of donor #1 and #2 with their future trajectories (arrows) estimated by RNA velocity analysis. **g** Pathway analysis of manually selected DC characteristics for the different clusters using gene set variation analysis (GSVA). Positive GSVA scores indicate an enrichment of strongly expressed genes in a pathway.

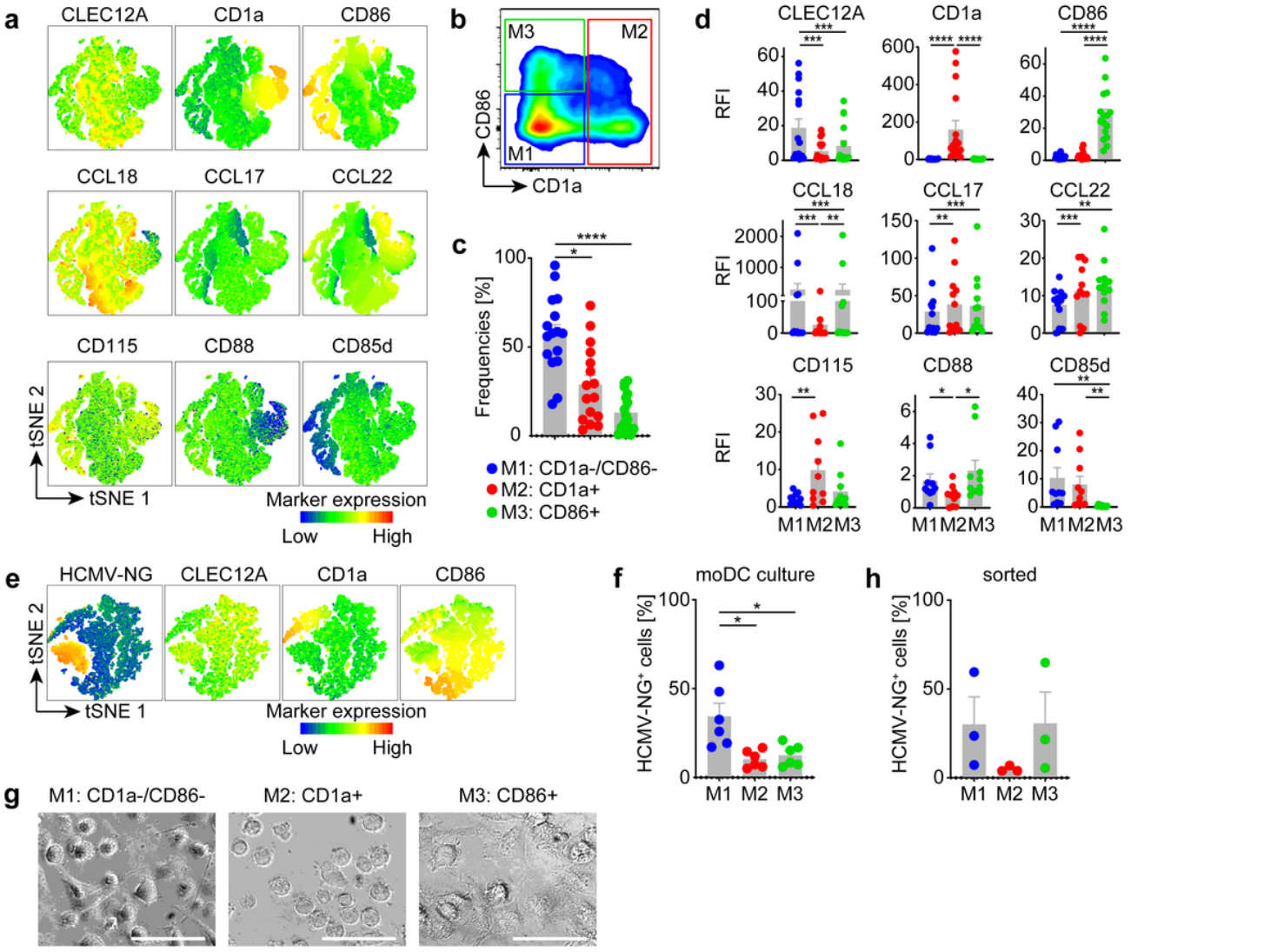

Fig. 3

Figure 3

moDCs comprise three subsets defined by characteristic protein expression profiles and differential susceptibilities to HCMV infection. moDCs were differentiated from 16 independent donors, and CLEC12A, CD1a, CD86, CCL18, CCL17, CCL22, CD115, CD88 and CD85d were immunolabeled and analyzed by flow cytometry. **a** tSNE plot of live cells showing heatmap coloring to indicate the abundance of each of the immunolabeling markers, data of one representative donor are shown. **b** Mock-exposed moDCs were immunolabeled as described above and the three moDC subsets were discriminated by gating of $CD1a^-/CD86^-$ (M1), $CD1a^+$ (M2) and $CD86^+$ (M3) cells. **c** Frequencies and **d** relative fluorescence intensities (RFI) of each of the analyzed markers in the three subset gates were determined. **e, f** moDCs were infected with HCMV-NG, immunolabeled and analyzed as above (a). tSNEs of NG fluorescence and the 3 most discriminative markers, i.e., CD1a, CD86, and CLEC12A (**e**) and percentages of NG^+ cells in each of the subsets are shown (**f**). **g** Mock-exposed moDC subsets were sorted using the gating strategy shown in (b) and analyzed morphologically (scale bar 50 µm). **h** Cells sorted as in (g) were infected with HCMV-NG and percentages of NG^+ cells were determined 24 hpi. Data represent mean±SEM of 7

independent experiments. Each dot represents a single donor. ****: p≤0.0001, ***: p≤0.0010, **: p≤0.0093, *: p≤0.0313 using two-tailed paired Wilcoxon signed-rank test.

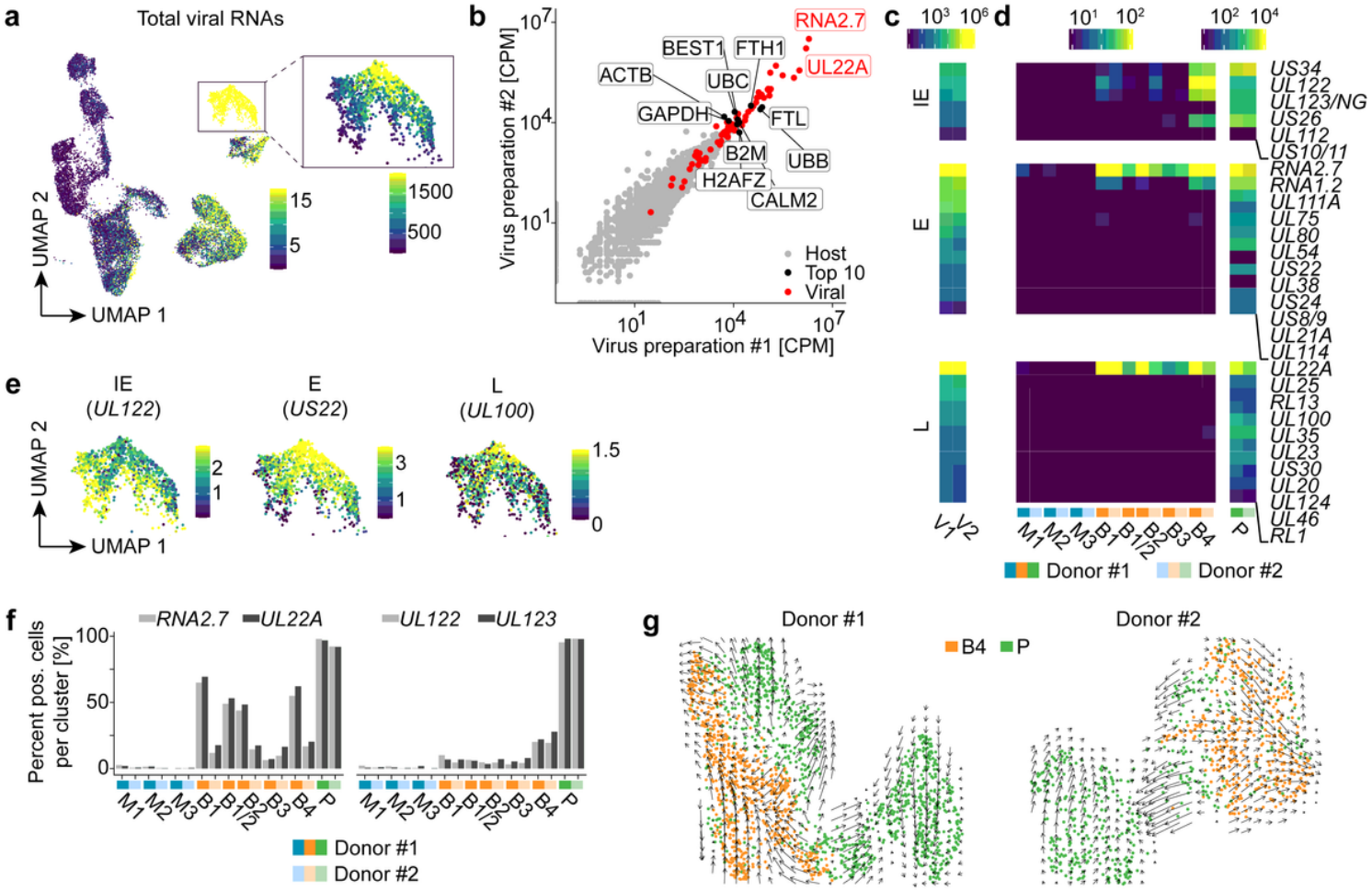

Fig. 4

Figure 4

Most HCMV-NG exposed moDCs contain virion-associated transcripts, but only few ones show *de novo* viral gene expression. a UMAP embedding showing total expression of viral RNAs (SCTransform normalized values) in the dataset analyzed also in Fig. 1. **b** Scatter plot showing the abundance of host (grey dots) and viral (red dots) RNAs (in counts per million) in the two independent virus preparations. The two most abundant viral RNAs (*RNA2.7, UL22A*) and the ten most abundant host RNAs (black dots) are labeled. **c, d** Heatmap showing the abundance of viral RNAs in the virus preparations V1 and V2 (**c**) and in the clusters detected by scRNA-seq (**d**) (counts per million). **e** IE genes are significantly more expressed in B4 than in B1-3 (p<3.5e-57, two-sided Wilcoxon rank sum test) UMAP embeddings depicting the expression (SCTransform normalized values) of representative viral RNAs of the different kinetic classes of HCMV gene expression in P. **f** Bar diagram showing differences in the abundance of virion-associated (*RNA2.7 and UL22A*) and *de novo* transcribed (*UL122 and UL123*) viral transcripts in mock

and HCMV-NG exposed cells. **g** RNA-velocity analysis of bystander cells in B4 (orange colors) and productively infected cells in P (green). Arrows indicate future trajectories of the cells.

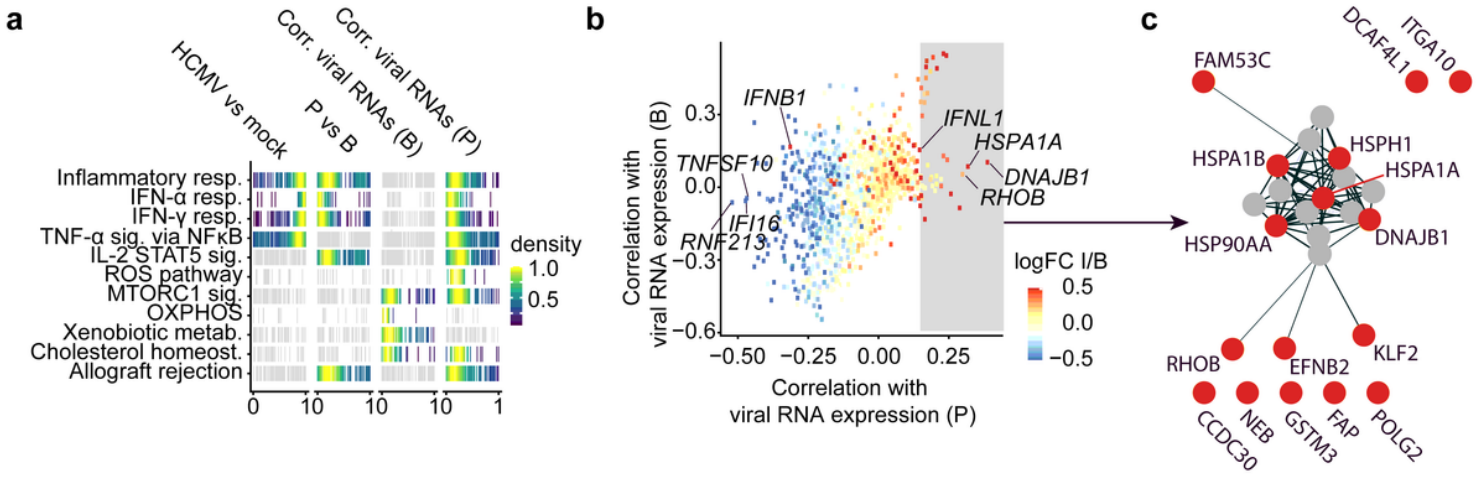

Fig. 5

Figure 5

Viral RNA expression is associated with decreased ISG and increased heat shock protein expression. a Pathway analysis (i) of differentially regulated genes in HCMV-NG versus mock-exposed (1st panel), (ii) of productively infected versus bystander moDCs (2nd panel), and (iii) correlation of host genes with viral RNA expression in bystander (3rd panel) and (iv) in productively infected moDCs (4th panel). Shown are all MSigDB Hallmark pathways in which at least one analysis was statistically significant (highlighted in color, p<0.01, two-sided Wilcoxon test, Benjamini-Hochberg multiple testing correction). Each vertical line is the rank of the fold change (1st and 2nd panel) or of the Spearman correlation (3rd and 4th panel) for a pathway gene. Colors represent kernel density estimates of ranks with the mode of the density scaled to 1. **b** Spearman's correlation coefficients between host transcript levels and viral RNA expression across bystander cells (B, y-axis) and productively infected cells (P, x-axis). Dots are colored depending on their

expression level in P relative to B (FC, fold change) revealing more down- (n=94) than upregulated (n=29) genes (Wilcoxon test, false discovery rate < 0.01, absolute $\log_2$ fold change >0.5). **c** Protein network derived from the 16 most positively correlated genes in HCMV-NG exposed clusters (highlighted in red). Connections represent predicted functional evidence for protein-protein interactions.

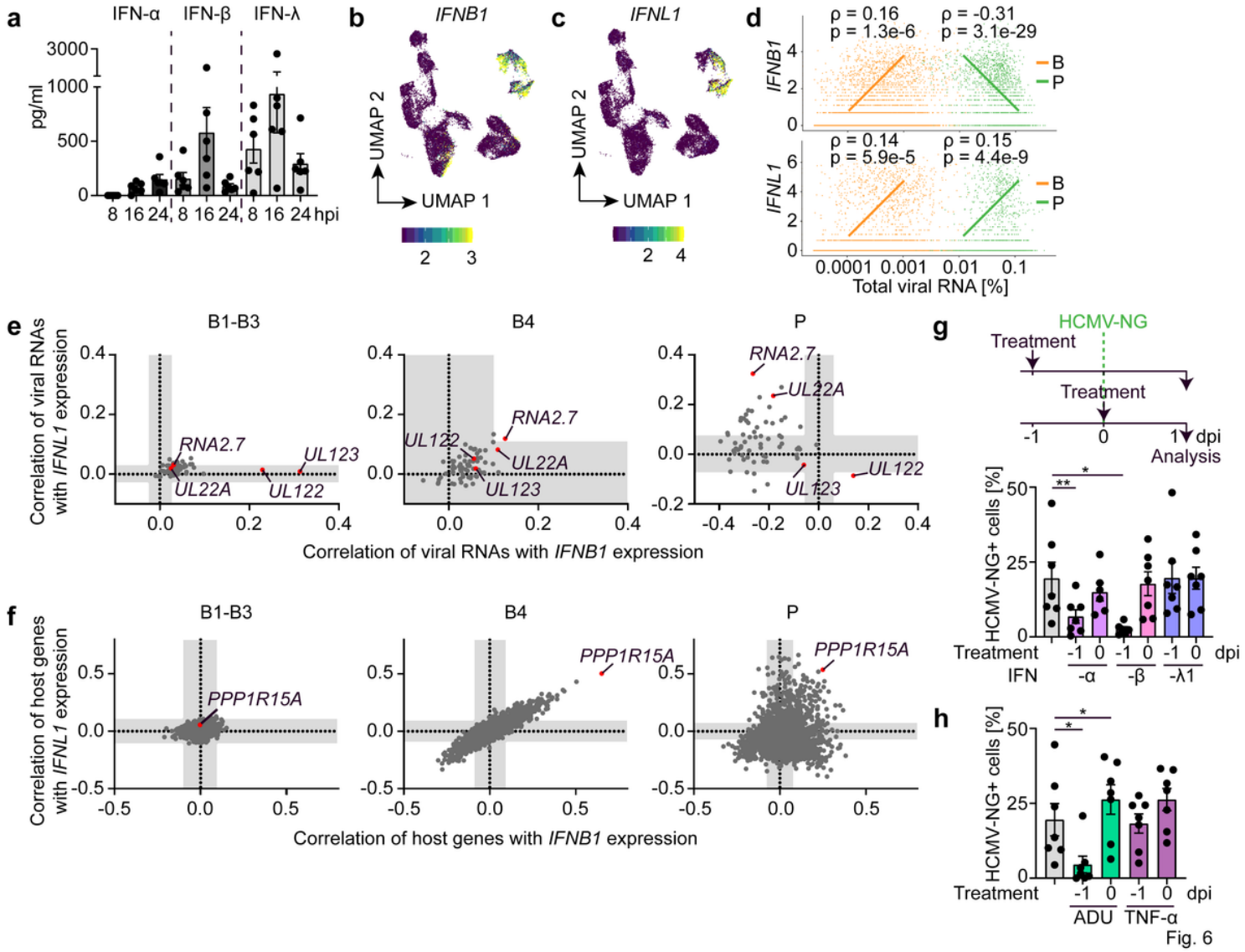

Figure 6

***IFNB1* correlates with viral IE gene expression, whereas progression of viral infection inhibits *IFNB1*, but not *IFNL1* induction. a** moDCs were exposed to HCMV-NG and supernatants were harvested completely and replenished with fresh medium 8, 16 and 24 hpi to determine the IFN-α, IFN-β or IFN-λ content by ELISA methods. **b, c** UMAP embeddings showing expression levels (SCTransform normalized values) of *IFNB1* (**b**) and *IFNL1* (**c**). **d** Expression (SCTransform normalized values) of *IFNB1* and *IFNL1* (y-axis) compared to total viral RNA abundance (x-axis, in percent relative to total feature counts per cell) in bystander (orange) and productively infected (green) cells. Values indicate Spearman's correlation coefficients as determined in Fig. 5b and lines visualize a positive or negative correlation. **e, f** Spearman´s

correlation coefficients of viral RNAs (**e**) and host genes (**f**) with *IFNB1* and *IFNL1* expression for clusters B1-3 (1st graph), B4 (2nd graph), and P (3rd graph). White areas indicate statistically significant regions (p<0.01, approximate t-test, Benjamini-Hochberg multiple testing correction). **g, h** moDCs were pre-treated at -1 days post infection (dpi) or treated at the time of HCMV-NG exposure (0 dpi) with IFN-α2b, IFN-β or IFN-λ1 (**g**) or ADU-S100 (ADU) and TNF-α (**h**) and percentages of NG^+ cells were quantified by flow cytometry. Values for HCMV-NG exposed cells without further treatment are the same in (**g**) and (**h**) as experiments were performed simultaneously. Mean ± SEM of 7 different donors from 3 independent experiments. Each dot represents a single donor. *: p≤0.0391, **: p≤0.0078 using one-tailed paired Wilcoxon signed-rank test.

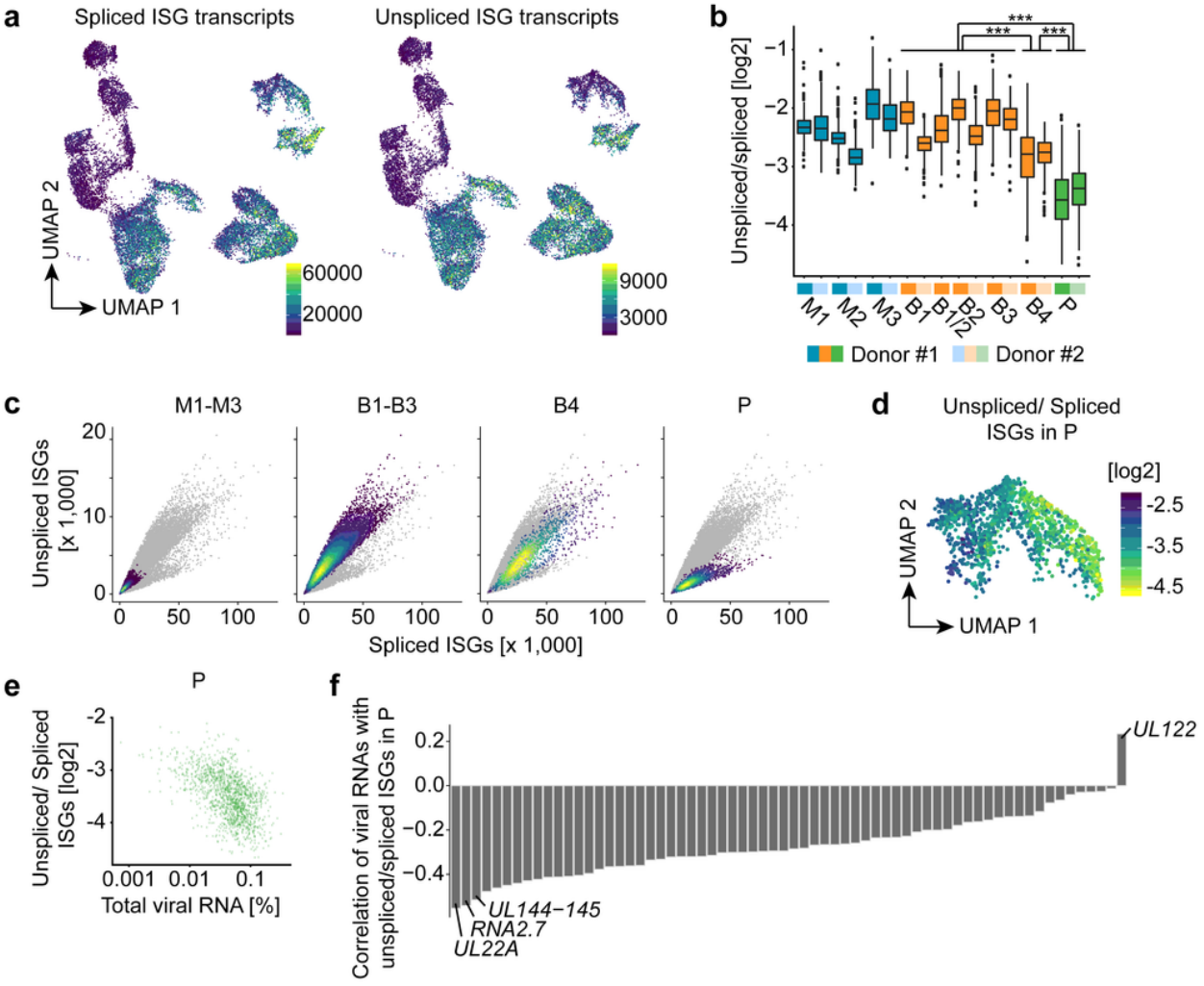

Fig. 7

Figure 7

Initial ISG transcription in productively infected cells is inhibited upon efficient viral gene expression. a UMAP embeddings highlighting the expression (raw feature counts) of spliced and un-spliced ISG transcripts. **b** Boxplots showing the distributions of unspliced vs. spliced fold changes for ISG transcripts

in all clusters (***: p<2.22e-16, two-sided Wilcoxon ranks-sum test). **c** Phase portraits showing expression of unspliced (y-axis) and spliced (x-axis) ISG transcripts per cell. Cells from clusters M1-3 (1st graph), B1-3 (2nd graph), B4 (3rd graph), and P (4th graph) are highlighted in color. **d** UMAP depicting the ratio of unspliced/spliced ISG transcripts per cell in P. **e** Unspliced/spliced ISG transcripts in P (y-axis) compared to total viral RNA expression (x-axis, in percent relative to total feature counts per cell). **f** Spearman's correlation coefficient for the ratio of unspliced/spliced ISG transcripts with the expression of single viral RNAs in P.

Supplementary Files

This is a list of supplementary files associated with this preprint. Click to download.

- SupplementaryTable1.xlsx
- SupplementaryTable2.xlsx
- SupplementaryTable3.xlsx
- SupplementaryTable4.xlsx
- Costaetal.SupplementaryFig.1.tif
- Costaetal.SupplementaryFig.2.tif
- Costaetal.SupplementaryFig.3.tif
- Costaetal.SupplementaryFig.4.tif
- Costaetal.SupplementaryFig.5.tif
- Costaetal.SupplementaryFig.6.tif